J|A|C|S
ARTICLES
Published on Web 02/27/2002

High Resolution Capillary Electrophoresis of Carbon Nanotubes

Stephen K. Doorn,*,† Robert E. Fields, III,† Hui Hu,‡,§ Mark A. Hamon,‡,§ Robert C. Haddon,‡,§ John P. Selegue,‡ and Vahid Majidi†

Contribution from the Chemistry Division (C-ACS, MS-J964), Los Alamos National Laboratory, Los Alamos, New Mexico 87545, and Department of Chemistry, University of Kentucky, Lexington, Kentucky 40506-0055

Received October 15, 2001

Abstract: Purification of single-walled carbon nanotubes by capillary electrophoresis (CE) is demonstrated. Real-time Raman spectroscopy of the separation process and single-wavelength UV/vis detection show the ability of CE to provide high-resolution separations of nanotube fractions with baseline separation. AFM images of collected fractions demonstrate that separations are based on tube length. The separation method is suggested to be based on alignment of the nanotubes along the separation field.

Introduction

The physical and chemical properties of carbon nanotubes are of great interest for potential applications in high-strength/lightweight materials and nanoscale electronics,[1] sensors,[2] and hydrogen storage,[3−5] among other areas. Pursuit of these applications is hampered by a lack of means to produce bulk quantities of pure materials. Much progress has been made in production methods, including DC-arc,[6] laser ablation,[7] and catalytic gas-phase growth.[8] These methods typically produce 50%−95% yields of nanotubes, with the mass balance consisting of amorphous carbon, graphitic material, and fullerenes. The nanotubes produced may vary in length, diameter, and structure. Many of their interesting properties are dependent on these structural parameters, and structure-based purification will be an important tool for advancing nanotube science.

Solvent (CS_2, toluene) treatment of raw nanotube material followed by ultrafiltration[9,10] is able to reduce to some degree the amount of non-nanotube material in the recovered samples. Flocculation using aqueous surfactants has also been investigated.[11,12] Use of oxidation and acid washing, coupled with (to varying degrees) centrifugation, resuspension in surfactant solution, and cross-flow filtration steps, has provided material of relatively high purity.[12−14] For all these methods, however, the final material is a mixture of tubes of differing lengths that still contains potential contamination with non-nanotube material. Polymer suspensions[15,16] and chromatographic purification[17,18] have proven useful at removing non-nanotube material. Field-flow fractionation on purified, shortened nanotubes[19] and size-exclusion chromatography on raw nanotubes suspended in SDS[20,21] have demonstrated some success at producing fractions separated by length. Each fraction, however, is a distribution of nanotubes of varying length, and fractions eluted at long times may contain non-nanotube material.

* To whom correspondence should be addressed. E-mail: skdoorn@lanl.gov.
† Los Alamos National Laboratory.
‡ University of Kentucky.
§ Current Address: Departments of Chemistry and Chemical and Environmental Engineering, University of California, Riverside, CA 92521-0403.

(1) Yakobson, B. I.; Smalley, R. E. *Am. Sci.* **1997**, *85*, 324.
(2) Kong, J.; Franklin, N. R.; Zhou, C.; Chapline, M. G.; Peng, S.; Cho, K.; Dai, H. *Science* **2000**, *287*, 622.
(3) Dillon, A. C.; Jones, K. M.; Bekkedahl, T. A.; Kiang, C. H.; Bethune, D. S.; Heben, M. J. *Nature* **1997**, *386*, 377.
(4) Chen, P.; Wu, X.; Lin, J.; Tan, K. L. *Science* **1999**, *285*, 91.
(5) Liu, C.; Fan, Y. Y.; Liu, M.; Cong, H. T.; Cheng, H. M.; Dresselhaus, M. S. *Science* **1999**, *286*, 1127.
(6) Journet, C.; Maser, W. K.; Bernier, P.; Loiseau, A.; Lamy de la Chapelle, M.; Lefrant, S.; Deniard, P.; Lee, R.; Fischer, J. E. *Nature* **1997**, *388*, 756.
(7) Thess, A.; Lee, R.; Nikolaev, P.; Dai, H.; Petit, P.; Robert, J.; Xu, C.; Lee, Y. H.; Kim, S. G.; Rinzler, A. G.; Colbert, D. T.; Scuseria, G. E.; Tomanek, D.; Fischer, J. E.; Smalley, R. E. *Science* **1996**, *273*, 483.
(8) Nikolaev, P.; Bronikowski, M. J.; Bradley, R. K.; Rohmund, F.; Colbert, D. T.; Smith, K. A.; Smalley, R. E. *Chem. Phys. Lett.* **1999**, *313*, 91.
(9) Bandow, S.; Rao, A. M.; Williams, K. A.; Thess, A.; Smalley, R. E.; Ecklund, P. C. *J. Phys. Chem. B* **1997**, *101*, 8839.
(10) Tohji, K.; Takahashi, H.; Shinoda, Y.; Shimizu, N.; Jeyadevan, B.; Matsuoka, I.; Saito, Y.; Kasuya, A.; Ito, S.; Nishina, Y. *J. Phys. Chem. B* **1997**, *101*, 1974.
(11) Bonard, J.-M.; Stora, T.; Salvetat, J.-P.; Maier, F.; Stockli, T.; Duschl, C.; Forro, L.; deHeer, W. A.; Chatelain, A. *Adv. Mater.* **1997**, *9*, 827.
(12) Rinzler, A. G.; Liu, J.; Dai, H.; Nikolaev, P.; Huffman, C. B.; Rodriguez-Macias, F. J.; Boul, P. J.; Lu, A. H.; Heymann, D.; Colbert, D. T.; Lee R. S.; Fischer, J. E.; Rao, A. M.; Eklund, P. C.; Smalley, R. E. *Appl. Phys. A: Mater. Sci. Process.* **1998**, *67*, 29.
(13) Dillon, A. C.; Gennett, T.; Jones, K. M.; Alleman, J. L.; Parilla, P. A.; Heben, M. J. *Adv. Mater.* **1999**, *11*, 1354.
(14) Li, F.; Cheng, H. M.; Xing, Y. T.; Tan, P. H.; Su, G. *Carbon* **2000**, *38*, 2041.
(15) Yudasaka, M.; Zhang, M.; Jabs, C.; Iijima, S. *Appl. Phys. A: Mater. Sci. Process.* **2000**, *71*, 449.
(16) Coleman, J. N.; Dalton, A. B.; Curran, S.; Rubio, A.; Davey, A. P.; Drury, A.; McCarthy, B.; Lahr, B.; Ajayan, P. M.; Roth, S.; Barklie, R. C.; Blau, W. J. *Adv. Mater.* **2000**, *12*, 213.
(17) Holzinger, M.; Hirsch, A.; Bernier, P.; Duesberg, G. S.; Burghard, M. *Appl. Phys. A: Mater. Sci. Process.* **2000**, *70*, 599.
(18) Niyogi, S.; Hu, H.; Hamon, M. A.; Bhomik, P.; Zhao, B.; Rozenzhak, S. M.; Chen, J.; Itkis, M. E.; Meier, M. S.; Haddon, R. C. *J. Am. Chem. Soc.* **2001**, *123*, 733.
(19) Liu, J.; Rinzler, A. G.; Dai, H.; Hafner, J. H.; Bradley, R. K.; Boul, P. J.; Lu, A.; Iverson, T.; Shelimov, K.; Huffman, C. B.; Rodriguez-Macias, F.; Shon, Y.-S.; Lee, T. R.; Colbert, D. T.; Smalley, R. E. *Science* **1998**, *280*, 1253.
(20) Duesberg, G. S.; Muster, J.; Krstic, V.; Burghard, M.; Roth, S. *Appl. Phys. A: Mater. Sci. Process* **1998**, *67*, 117.
(21) Duesberg, G. S.; Blau, W.; Byrne, H. J.; Muster, J.; Burghard, M.; Roth, S. *Synth. Met.* **1999**, *103*, 2484.

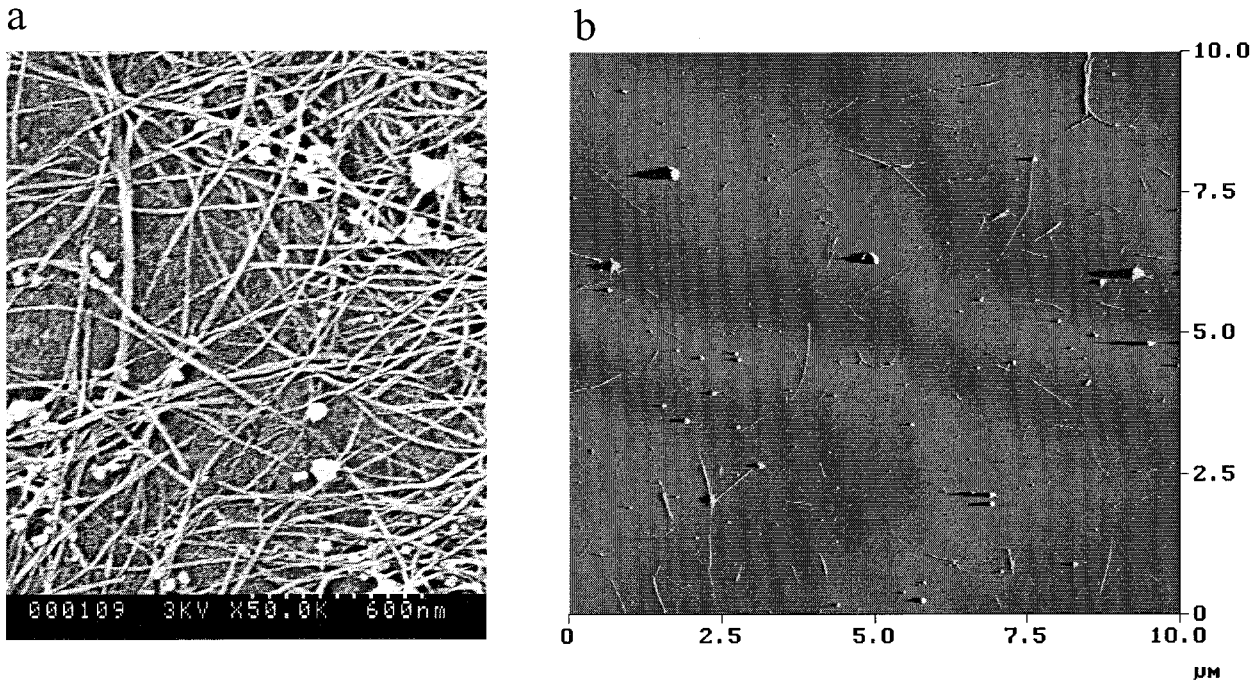

Figure 1. (a) SEM image of single-walled carbon nanotubes (raw mat) used for the separations study. The sample consists of tubes of varying lengths intermixed with carbonaceous impurities. (b) AFM image of single-walled carbon nanotubes used for the separations study (dispersed in DMF).

Electrophoretic methods have shown potential for purification of nanotubes. Bulk electrophoresis has been used for alignment of nanotubes and is capable of separating nanotubes from particulate impurities.[22] We demonstrate here the use of capillary electrophoresis (CE) as an alternative method for separating carbon nanotubes by size. CE separations are based on charge- and size-dependent mobility of solution phase species under the influence of an applied electric field. The rapid, high-resolution separations available with CE have the potential to separate a nanotube sample into discrete fractions of uniformly sized tubes.

Experimental Section

The carbon nanotubes used in this study are single-walled nanotubes (SWNTs) prepared using the modified electric-arc method.[6] An SEM image of the resultant raw nanotube mat, obtained with an Hitachi S900 field-emission SEM, is shown in Figure 1a. The raw nanotubes are purified using nitric acid oxidation, followed by the centrifugation, resuspension, and cross-flow filtration steps described in refs 12 and 19. Atomic force microscopy (AFM) images (such as shown in Figure 1b) of this initially purified material were taken from nanotubes suspended in DMF and subsequently deposited and dried on the substrate. AFM images were obtained with a Digital Instruments nanoscope. All AFM samples were prepared on mica substrates. Imaging was performed in tapping mode.

Samples used for the CE separations studies are 0.83 mg/mL of SWNTs suspended through ultrasonication with a horn sonicator in an aqueous solution of 0.5% sodium dodecyl sulfate (SDS). This is slightly above the critical micelle concentration (cmc) for SDS (0.24%) and has been shown to efficiently suspend carbon nanotubes while minimizing their aggregation.[11,23] SDS has been shown previously to provide the basis for separation of other carbon materials (fullerenes) in micellar electrokinetic chromatography (MEKC).[24] For SWNT separations, however, the use of a micellar medium such as SDS does not have the same significance as in a MEKC application. MEKC relies on partitioning of a neutral solute into the micelle.[25] The SWNTs are too large to reside in the intramicellar region. Instead, the hydrophobic SDS tails are expected to specifically interact with the nanotube surface, providing it with a negative charge.[23] The resultant electrostatic repulsion between tubes stabilizes them against van der Waals attraction. Investigations into the phase behavior of the SDS/SWNT/water system show that, for the relative concentration of SDS and SWNTs at which we are working, a stable single-phase dispersion of nanotubes results.[23]

CE with absorbance detection at 360 nm was performed on a commercial instrument, using a 75 μm inside diameter, 1 m long fused silica capillary with detection window located at 75 cm from the sample intake. The capillary was conditioned for 2 min using 0.2 M NaOH, followed by flushing with deionized water and buffer solution. The run buffer was 50 mM trizma base in 0.5% SDS solution. The sample was pressure-loaded at 100 mbar for 30 s before applying the separation voltage of +15 kV. The positive potential is applied to the capillary input (anode) and retards the flow of negatively charged species with respect to the net electro-osmotic flow toward the capillary output (cathode).

CE with Raman detection was performed with a lab-built CE apparatus. CE parameters were the same as for the absorbance detection experiments, with Raman detection at 25 cm from the intake end of a 1 m capillary. Sample introduction was done by pulling sample into the capillary with a syringe for 2 s. An initial syringe void volume of 1 mL was increased to 3 mL for the 2 s uptake time. The resultant uptake pressure was approximately 500 mbar. Spectra were collected continuously in real time through a confocal Raman microscope during the course of the separation; 5 mW of 514.5 nm light was line-focused (approximately 1 μm wide by 50 μm long) into the center of the capillary (along its axis) using a 20× (NA 0.4) microscope objective. Scattered light was collected into a Kaiser Optical HoloSpec f/1.8 imaging spectrograph. A 50 μm entrance slit resulted in 4 cm^{-1} spectral resolution. Detection was with a front-illuminated Princeton Instruments CCD camera (1024 × 256 pixels) using 1 s integration times.

(22) Yamamoto, K.; Akita, S.; Nakayama, Y. *J. Phys. D: Appl. Phys.* **1998**, *31*, 34.
(23) Vigolo, B.; Penicaud, A.; Coulon, C.; Sauder, C.; Pailler, R.; Journet, C.; Bernier, P.; Poulin, P. *Science*, **2000**, *290*, 1331.
(24) Treubig, J. M., Jr.; Brown, P. R. *J. Chromatogr. A* **2000**, *873*, 257.
(25) Weinberger, R. *Practical Capillary Electrophoresis*; Academic Press: San Diego, 2000.

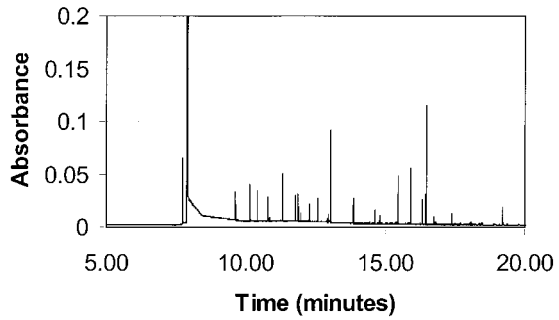

Figure 2. Capillary electropherogram of single-walled carbon nanotubes using absorbance detection at 360 nm. Run taken at +15 kV in 0.5% SDS/50 mM trizma base buffer.

Results and Discussion

AFM analysis of the SWNTs demonstrates that the sample used for CE separations is a mixture of tubes ranging in length primarily from around 75 nm to 2 μm (Figure 1b). Some non-nanotube impurities are also present. Results from a typical CE separation using absorbance detection are shown in Figure 2. Fractions begin to appear around 8 min into the run. From run-to-run, we consistently observe an initial strong sharp peak on top of a broad background followed by a series of sharp peaks. These peaks are typically only 1−2 s in width. Note also the baseline separation of closely occurring peaks. Elution times are also observed to compare well with what can be obtained from CE separations on other types of analytes. Depending on analyte and separation parameters, typical elution times can range from as short as 1 min to 20 min.[25] We believe the sharp peaks in the electropherogram are due to nanotube fractions. Because of the potential presence of other material (such as fullerenes and graphite), however, unambiguous identification of these peaks requires Raman detection.

A Raman/CE run showing total detected intensity at 560.37 nm (corresponding to the strong nanotube Raman band at 1591 cm^{-1}) is shown in Figure 3a.[26] We observe a similar pattern to that seen in the absorbance data. Initial sharp bands appear superimposed on a broad fluorescence background, followed by a series of trailing peaks. In the Raman detection case, the first bands observed appear a factor of 3 times earlier than observed for absorbance detection. This is consistent with a detection region that is 3 times closer to the intake end of the capillary for Raman detection. Run-to-run changes in the number of observed fractions and their positions are observed. This is most likely due to the heterogeneous nature of the nanotube suspension, which can result in sampling differences between runs. No Raman bands are associated with the broad fluorescence feature, nor are any observed for any other point in the electropherogram, except at the location of the sharp bands. Strong Raman bands, characteristic of carbon nanotubes, are observed for all the sharp features in the electropherogram, giving positive identification of these fractions as containing nanotubes. A sample Raman spectrum from an individual fraction is shown in Figure 4. Subtraction of the base intensity from the peak intensity at 1591 cm^{-1} results in an electropherogram that displays only the carbon nanotube fractions (Figure 3b).

The spectrum in Figure 4 shows five Raman bands. The band at 169 cm^{-1} is the nanotube breathing or radial mode and is strongly dependent on the tube diameter.[27] (This band is typically higher in relative intensity, but is attenuated in our spectrum

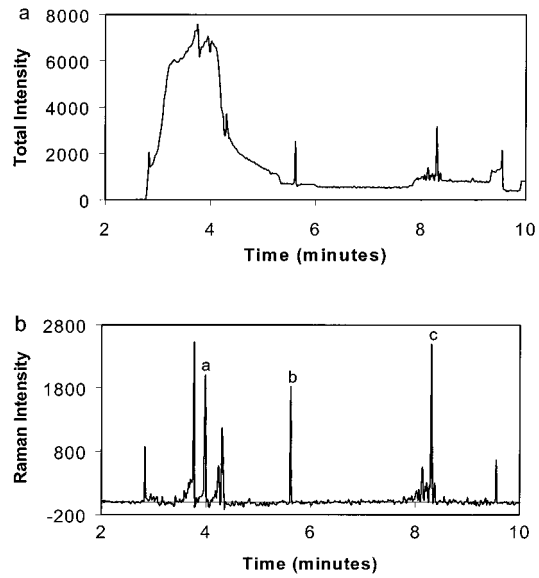

Figure 3. Capillary electropherograms of single-walled carbon nanotubes using Raman detection. Run taken at +15 kV in 0.5% SDS/50 mM trizma base buffer. (a) Electropherogram showing total intensity (background fluorescence plus Raman scattering) collected at 560.37 nm. (b) Electropherogram showing scattered Raman intensity at 1591 cm^{-1}.

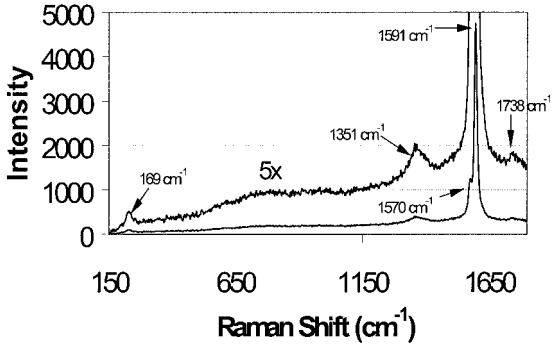

Figure 4. Raman spectrum of an individual single-walled carbon nanotube fraction.

due to the notch filter used with the Raman microscope.) The bands at 1591 and 1570 cm^{-1} correspond to in-plane deformations, while the band at 1351 cm^{-1} is assigned as a defect mode that arises from breaking the translational symmetry of a graphene sheet to form the cylindrical nanotube.[28] The weak band at 1738 cm^{-1} appears to be a combination mode arising from the 1570 and 169 cm^{-1} modes. The spectrum is consistent with that expected for a mixture of semiconducting and metallic single-walled nanotubes[27] with a diameter of 1.32 nm.[29]

The pure nanotube electropherogram (Figure 3b), even with a factor of 3 faster elution than used in the absorbance experiments, still shows baseline separation of discrete nanotube fractions. The bands are typically the width of our integration time (1 s), with some of the stronger bands being up to 2−3 s wide. The sharpness of these bands may be due to a number of

(26) Although the electropherograms obtained with Raman detection are presented for only one wavelength, we wish to emphasize that each point in the electropherogram actually represents a complete Raman spectrum for that segment (fraction) of sample flowing through the capillary.
(27) Rao, A. M.; Richter, E.; Bandow, S.; Chase, B.; Eklund, P. C.; Williams, K. A.; Fang, S.; Subbaswamy, K. R.; Menon, M.; Thess, A.; Smalley, R. E.; Dresselhaus, G.; Dresselhaus, M. S. *Science* **1997**, *275*, 187.
(28) Eklund, P. C.; Holden, J. M.; Jishi, R. A. *Carbon* **1995**, *33*, 959.
(29) Bandow, S.; Asaka, S.; Saito, Y.; Rao, A. M.; Grigorian, L.; Richter, E.; Eklund, P. C. *Phys. Rev. Lett.* **1998**, *80*, 3779.

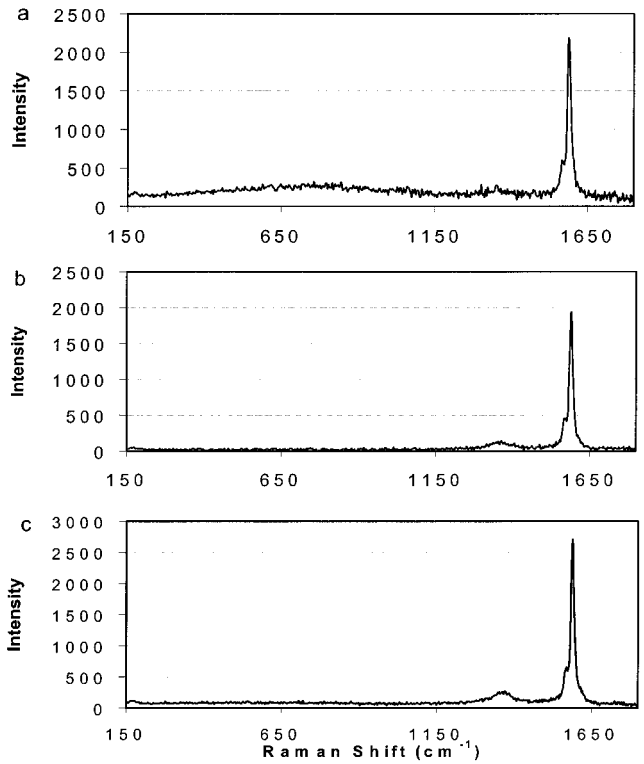

Figure 5. Raman spectra of labeled fractions from capillary electropherogram shown in Figure 3: (a) 3.98 min fraction, (b) 5.62 min fraction, (c) 8.30 min fraction.

factors, including reduced interaction with the capillary walls due to the presence of surfactant, the purity of individual nanotube fractions, the stability of the nanotubes, and the presence of only a small amount of material in any given fraction. This last point is supported by the observation that the most intense bands also tend to be the widest ones.

Raman spectra of three individual fractions (highlighted in Figure 3b) are compared in Figure 5. It is interesting to note that Raman frequencies are identical for all fractions, indicating that each fraction contains tubes of equivalent diameter. Although the radial mode is most sensitive to tube diameter, the 1591 cm^{-1} mode will experience small shifts (on the order of a few wavenumbers) as tube diameter changes.[27] Thus, band broadening and shoulders are commonly observed on the 1591/1570 cm^{-1} combination and for the 169 cm^{-1} band in samples of mixed tubes. These features are not present in our spectra, suggesting a high degree of uniformity in tube diameter within our sample. The arc method produces primarily nanotubes with diameters of about 1.3 nm,[30,31] so it is not surprising to find that all fractions in the electropherograms consist of tubes of similar diameter. This suggests that the difference in mobility between fractions is due to differences in nanotube lengths.

Further evidence for length-based separation was obtained from AFM images of collected fractions. We were unable to collect individual nanotube fractions but instead obtained AFM data from composite fractions collected at progressively later times during a separation. Composites were collected by turning off the separation voltage, followed by sectioning the capillary and then depositing and drying the section contents onto an AFM substrate. Each capillary section is comprised of a series of individual nanotube fractions occurring progressively later in time. The first composite encompassed sample that included the initial spikes and broad peak (see Figure 2). The second composite included the next two minutes of eluting fractions. Subsequent composites were obtained at approximately 5-min intervals. AFM images from the first two composites are shown in Figure 6. The first composite is found to consist of nanotubes ranging in length from 0.2 to 1.2 μm. Amorphous nonnanotube material was found only in the first composite. The second composite is found to consist of longer nanotubes (0.5−2.5 μm in length) with no amorphous material being present. The larger crystalline-like features found in these images are due to dried electrolyte and SDS.

Table 1. Range of Nanotube Lengths Observed in Composite Fractions

composite no.	length range (μm)	composite no.	length range (μm)
1	0.2−1.2	3	2.0−4.0
2	0.5−2.5	4	1.8−10.0

Previous results on gel-permeation chromatography of soluble SWNTs show that Raman spectra of fractions containing only amorphous nanoparticulates are dominated by a strong fluorescence background.[18,32] This background is absent in Raman spectra of fractions containing only nanotubes. We observe a similar background in Raman spectra taken during the time frame that comprises the first composite (Figure 3a). Later composites encompass time frames that do not show this fluorescence background, nor do these later composites contain amorphous particulates. It is therefore likely that the amorphous material found in composite 1 is responsible for the broad fluorescence background (and broad absorbance peak—see Figure 2) observed at early times.

The trend toward longer nanotubes continues in composites collected at later times (see Table 1). Some degree of overlap in length range between sequential composites is observed.

The significance of the overlap can be evaluated by measuring the distribution of lengths present in each composite. Figure 7 shows the distribution of nanotube lengths observed for the first four composites. Distributions were obtained through measurements made on three or four AFM images for each composite. It is found that the length range in which overlap occurs between composites contains a relatively small number of nanotubes compared to the length range into which the majority of tubes in each composite falls. This suggests that length range overlaps between composites result from diffusion of nanotubes between composites. Diffusion between composites is possible because of the time it takes to section the capillary after stopping the separation.

In the latest composites we observe lengths up to 10 μm, even though tubes longer than 2 μm are not observed in our raw nanotube sample. Bundling of individual tubes can result in the existence of longer structures. Although large-scale aggregation is prevented by the presence of SDS, small bundles are known to occur in these solutions. In addition to providing a pathway for producing longer tubes, bundling may also result in short aggregates with effectively larger diameter than

(30) Bethune, D. S.; Kiang, C. H.; deVries, M. S.; Gorman, G.; Savoy, R.; Vazquez, J.; Beyers, R. *Nature* **1993**, *363*, 605.
(31) Chen, J.; Hamon, M. A.; Hu, H.; Chen, Y.; Rao, A. M.; Eklund, P. C.; Haddon, R. C. *Science* **1998**, *282*, 95.
(32) Zhao, B.; Hu, H.; Niyogi, S.; Itkis, M. E.; Hamon, M. A.; Bhowmik, P.; Meier, M. S.; Haddon, R. C. *J. Am. Chem. Soc.* **2001**, *123*, 11673.

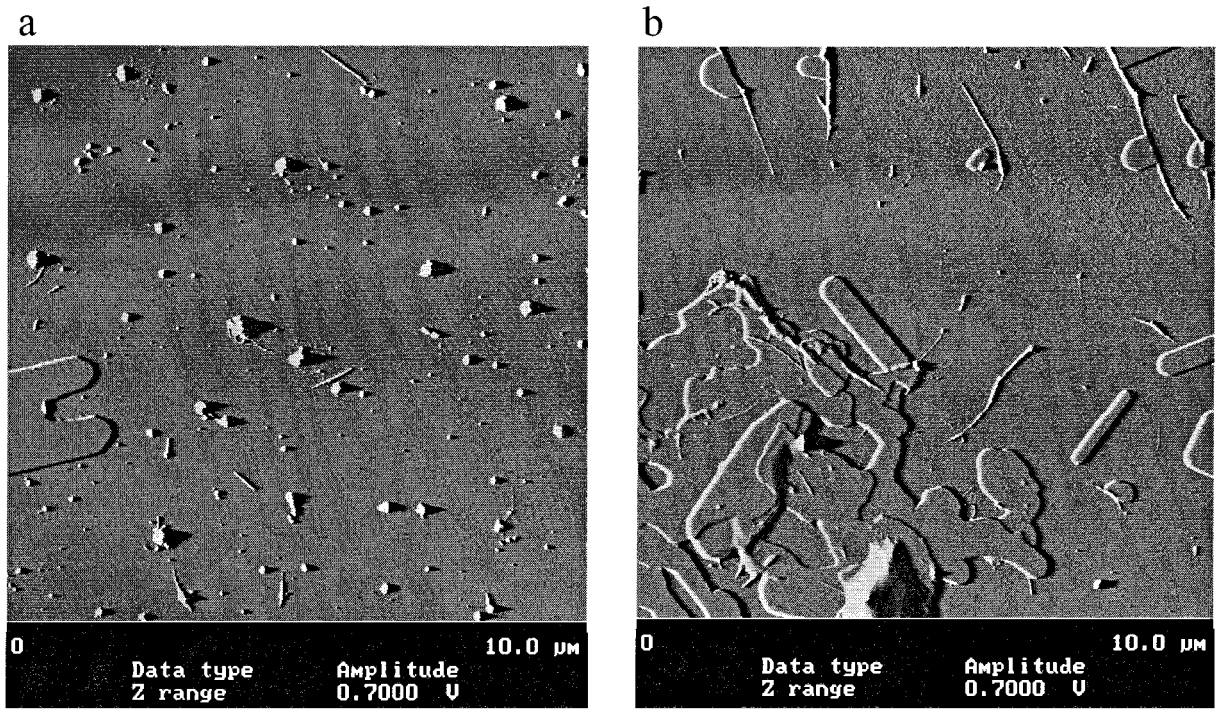

Figure 6. (a) AFM image of first (early time) composite of nanotube fractions. (b) AFM image of second composite of nanotube fractions.

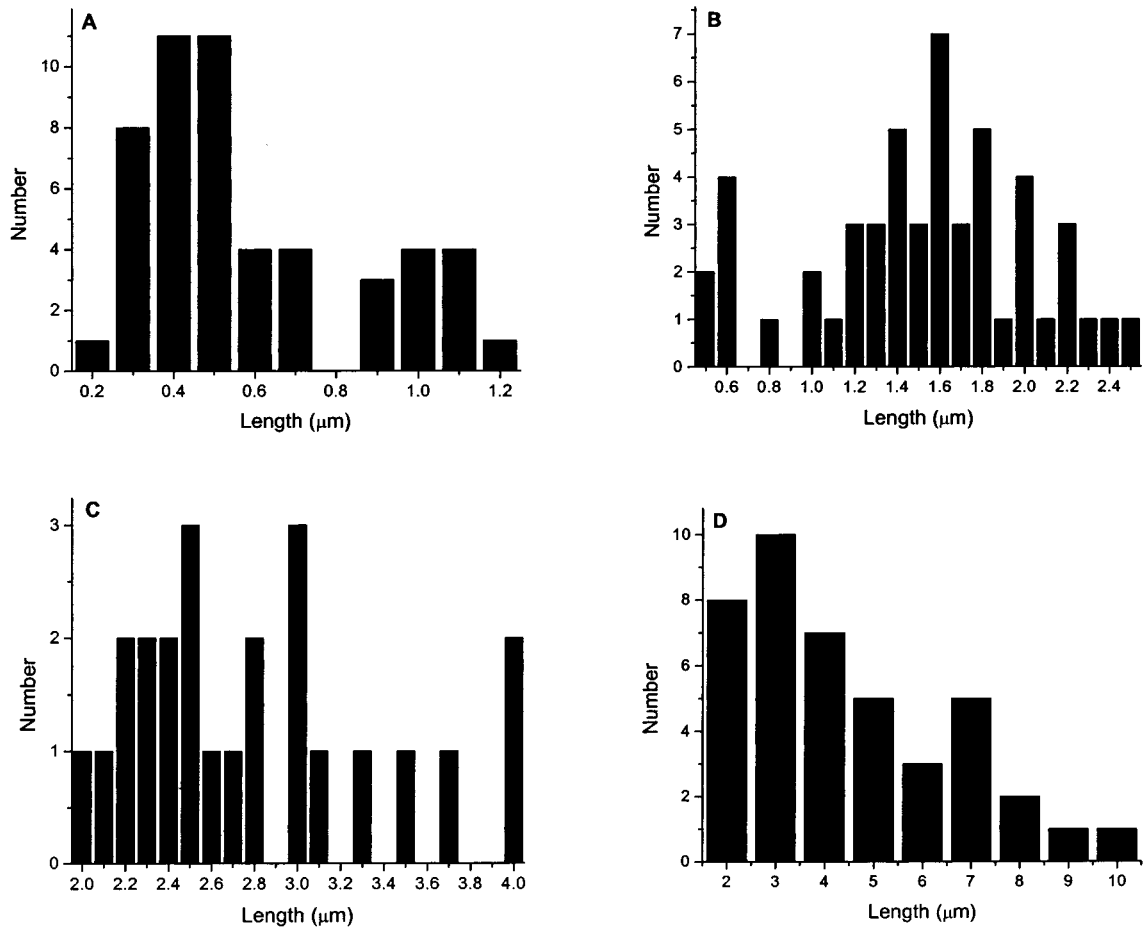

Figure 7. Distribution of nanotube lengths observed in each composite as determined from AFM images: (a) composite 1 (data from four images), (b) composite 2 (data from four images), (c) composite 3 (data from three images), (d) composite 4 (data from four images).

individual tubes. The existence of tubes as short as 2−3 μm in composite 4, although possibly present due to diffusion from composite 3, instead may be due to bundling of short tubes (the resolution of our AFM images does not allow differentiation

between bundled and individual tubes). Tube bundles of identical length to individual tubes will be expected to elute later due to their larger diameter (see later discussion).

The AFM results on composite fractions demonstrate a length-based separation mechanism that leads to elution of short tubes first, followed by progressively longer tubes. We propose the following mechanism for separation of nanotube fractions. SDS is expected to provide a negative charge to the nanotubes through specific interaction over the surface of the tubes. We find that nanotube fractions begin to appear shortly after elution of a neutral marker (methanol) of the electro-osmotic flow, confirming that the nanotubes carry a negative charge. The charge on the tubes will be proportional to their surface area. CE separations are based on differences in electrophoretic mobility between solutes: those having higher charge density have proportionately greater mobility. In the case of comparing elution times between individual tubes and tube bundles of the same length, the bundled tubes are expected to have a higher charge per unit length due to their greater diameter. The resultant higher electrophoretic mobility for the bundles is expected to translate to a later elution time than for an individual tube of identical length. For the case of nanotubes with uniform diameter, however, charge-density differences are not expected to be significant and forces other than electrophoretic ones are responsible for separations.

Under the influence of an electrostatic field (**E**), the nanotubes will experience an induced dipole moment ($\mathbf{p_x}$). The resultant torque on the nanotubes ($\mathbf{p_x} \times \mathbf{E}$) will align the tubes along **E**.[33] For perfectly aligned tubes of equal diameter, charge density along **E** will be the same, independent of length. It has been observed in bulk electrophoresis alignment experiments,[22] however, that shorter tubes display a larger deviation from perfect alignment than is observed for longer tubes. This behavior is predicted to occur as a result of opposition to alignment caused by Brownian motion or thermal agitation.[33] Shorter tubes are predicted to have a greater deviation from alignment along **E**. The resultant "wobble" is expected to effectively create a hydrodynamic resistance to the electrophoretic flow that will increase as tube length decreases. Under a positively applied potential, the negatively charged tubes will be attracted to the anode, or capillary intake, with longer tubes being most strongly attracted due to decreased hydrodynamic resistance resulting from their greater alignment along the applied electric field. Because there is a net flow toward the capillary outlet (cathode) for all species due to electro-osmotic flow, however, the tubes will still ultimately flow toward the cathode, but it is expected that the shorter tubes will elute first.

Confirmation of this proposed mechanism will rely in part on more detailed AFM analysis of individual SWNT fractions. Isolation of individual fractions may be possible through electrodeposition into wells that are micropatterned onto an AFM substrate. These collection wells could be generated through microcontact printing techniques. Development of this capability will also be of great interest for isolating tubes with known physical parameters for later use.

Conclusion

In conclusion, we have demonstrated the first use of CE for purification of carbon nanotubes. The high-resolution separations available with CE allow for separation of tubes into discrete fractions according to tube length. CE is also effective at removing non-nanotube material. These results represent an important improvement in size selectivity over that currently available with size-exclusion chromatography or field-flow fractionation. Because total tube charge and charge density is ultimately dependent on tube diameter, this approach is expected to be effective at separating tubes based on diameter as well. Diameter-dependent mobility may hold some potential for separations of chiral tubes from those with armchair or zigzag configuration. Studies in support of this potential require a more diverse mixture of tube diameters than used in this work and will be the subject of future investigations. The strong charge density dependence for CE separations may also make possible purification dependent on shape, allowing for collection of kinked or spiral tubes. The potential this technique has for isolating tubes of a specific desired property makes this an attractive area for further study.

Acknowledgment. Work at Los Alamos was supported by internal LDRD funding. Raman microscopy was performed at LANL's Integrated Spectroscopy Laboratory. The work at the University of Kentucky was supported by the Office of Naval Research under Award Number N00014-99-1-0770 and by the MRSEC Program of the National Science Foundation under Award Number DMR-9809686 and the U.S. Department of Energy under Award Numbers DE-FG02-00ER45847 and subcontract 10186-00-23.

JA012364C

(33) Fishbine, B. H. *Fullerene Sci. Technol.* **1996**, *4*, 87.